University of Sistan and Baluchestan

Challenges in Nano and Micro Scale Science and Technology

Online ISSN: 2821 - 000X

Magnetic Nanoparticle Hyperthermia for Peritoneal Metastasis-Impact of Tumor Location and Abdominal Fat

Mohadese Ranjbaran[1] | Mohammad Hossein Tavakoli[2] | Zahra Keshtpour Amlashi[3] | Safoora Nikzad[4]

1. Department of Physics, Faculty of Science, Bu-Ali Sina University, Hamadan 65174, I.R. Iran.
2. Corresponding Author, Department of Physics, Faculty of Science, Bu-Ali Sina University, Hamadan 65174, I.R. Iran. Email: mht@basu.ac.ir
3. Cancer Research Center, University of Medical Sciences, Hamadan 65178, I.R. Iran.
4. Department of Medical Physics, Faculty of Medicine, University of Medical Sciences, Hamadan 65178, I.R. Iran.

Article Info

Article type:
Research Article

Keywords:
magnetic nanoparticles,
hyperthermia,
peritoneal metastasis,
magnetic field,
cancerous tumor

ABSTRACT

Objective: This study investigates the impact of magnetic hyperthermia on the treatment of peritoneal metastases and analyzes the effects of abdominal fat and tumor position. The primary objective is to assess the effectiveness of localized heating with magnetic fields in eliminating cancer cells while minimizing damage to healthy tissue.

Method: In this study, magnetic nanoparticles Fe_3O_4 were used to increase the temperature of tumor tissues to the range of 42-46 °C under the influence of an alternating magnetic field. A numerical simulation using the finite element method was conducted to analyze the impact of abdominal fat and tumor position on heat transfer, and the distribution of magnetic field intensity was calculated using Maxwell's equations and the heat generated by nanoparticles based on Rosensweig's theory. In this study, the heat generated by nanoparticles in the tumor has been incorporated into the Pennes bioheat transfer equation, and the temperature distribution in the tumor and surrounding healthy tissues has been calculated.

Results: Magnetic hyperthermia effectively eliminates cancer cells and performs well in areas with thick abdominal fat, which are challenging, so abdominal fat does not hinder hyperthermia. The tumor's position significantly affects heat distribution, and more precise adjustments are needed in areas with higher metastasis. This method can be used alone or with other treatments.

INTRODUCTION

Cancer is one of the most significant challenges in human health today. This complex disease occurs when abnormal cells multiply uncontrollably in the body. These cells can invade nearby tissues and spread to other parts of the body through the bloodstream or lymphatic system, a process known as metastasis. When we describe cancer as aggressive, we mean that the cancer cells have invaded surrounding tissues or other organs, resulting in the formation of metastases [1–3]. Peritoneal metastasis usually originates from another organ and then spreads to the peritoneal cavity. It may arise from cancers of the stomach, intestines, colon, uterus, ovaries, or esophagus [4, 5]. Common cancer treatments such as chemotherapy, radiotherapy, and surgery are often used in combination to improve patient outcomes. However, a major challenge with these conventional methods is their inability to selectively target cancer cells without harming healthy tissues. The ideal cancer treatment would be one that effectively destroys cancer cells while minimizing damage to normal tissues. One promising advancement in non-invasive cancer treatment is hyperthermia, a technique that has recently gained acceptance and approval. This method involves controlled heating of tumor tissues to temperatures between 42–46°C, leading to the destruction of cancer cells. Hyperthermia is now being integrated with conventional treatments and has demonstrated a wide range of applications in medical science [6, 7]. In hyperthermia therapy, heat can be generated through various methods. One effective approach involves using magnetic nanoparticles (MNPs) in combination with an alternating magnetic field (AMF). In this method, MNPs act as localized heat sources, raising the temperature within the tumor. Accurate thermal analysis and precise

How to Cite this paper: Ranjbaran M. Tavakoli M.H. Keshtpour Amlashi Z. Nikzad S. Magnetic Nanoparticle Hyperthermia for Peritoneal Metastasis-Impact of Tumor Location and Abdominal Fat. *Challenges in Nano and Micro Scale Science and Technology*. 2024; 12(1): 48-57. DOI: 10.22111/cnmst.2025.52294.1263

© Ranjbaran M. Tavakoli M.H. Keshtpour Amlashi Z. Nikzad S. Publisher: University of Sistan and Baluchestan.

DOI: 10.22111/cnmst.2025.52294.1263

temperature distribution in both the tumor and surrounding healthy tissues are critical for the success of the treatment. Several factors influence this process, including the frequency, intensity, and spatial distribution of the magnetic field; the physical and chemical properties of the MNPs; the tumor's location; and the duration of treatment [8–11]. While numerous studies have explored the use of MNP-based hyperthermia for treating tumors in various parts of the body [12–16], research on its application for peritoneal metastases remains limited due to several challenges and obstacles. Overcoming these challenges is essential to advance treatment options for patients with peritoneal metastases and to improve their prognosis. Matsumi et al. experimentally investigated the treatment of peritoneal metastasis originating from gastric cancer using a mouse model. For treatment, they employed magnetic hyperthermia therapy (MHT) with superparamagnetic iron oxide (Fe_3O_4) nanoparticles (SPIONs). Their findings demonstrated that MHT is more effective for treating peritoneal metastases compared to other conventional treatments. Based on this study, MHT shows promise as a novel therapeutic option for peritoneal metastasis [17]. Magnetic nanoparticle hyperthermia requires an induction coil to generate the alternating magnetic field (AMF) necessary for heat production [18–21].

Rouni et al. evaluated the safety of magnetic hyperthermia systems utilizing nanoparticles to generate controlled heat for cancer treatment. Their research focused on assessing the safety of systems combining AMF and magnetic nanoparticles (MNPs) through practical experiments and empirical data, particularly regarding their impact on body temperature [22].

Chia et al. examined the effects of hyperthermia, both alone and in combination with intraperitoneal drug delivery, in treating peritoneal metastases. Their study initially assessed the immune status of the healthy peritoneal cavity and the immune microenvironment of peritoneal metastases. Subsequently, they analyzed the positive and negative impacts of hyperthermia and its heat shock response on the tumor immune microenvironment. Furthermore, they investigated how hyperthermia influences the biomechanical properties of tumor tissue and its effects on immune cell infiltration [23]. In addition to SPIONs, several other materials have been utilized in hyperthermia treatments, including various types of magnetic nanoparticles (MNPs) such as cobalt, nickel, and core-shell nanoparticles. Each material possesses unique properties that make it suitable for generating localized heat when exposed to an alternating magnetic field (AMF). The choice of material affects critical factors such as heat generation efficiency, biocompatibility, and magnetic response, all of which are essential for optimizing treatment effectiveness while minimizing adverse effects [24–26].

In this study, we used SPIONs due to their superior efficacy in treating peritoneal metastasis. Matsumi et al.'s experimental findings demonstrated that these nanoparticles generate localized heat more effectively under AMF exposure, making them especially suitable for targeting metastatic tumors in sensitive areas like the peritoneum. Their ability to selectively heat tumor cells while sparing surrounding healthy tissue enhances overall treatment outcomes [17]. SPIONs also offer improved thermal and magnetic stability, increasing heating efficiency during hyperthermia treatment. These nanoparticles provide greater safety by reducing risks such as clot formation or accumulation in non-target tissues. Additionally, SPIONs produce effective heat upon exposure to AMF, enabling controlled destruction of cancer cells. Their uniform dispersion in biological environments contributes to better thermal distribution and improved therapeutic efficacy. These properties make SPIONs a promising and effective choice for magnetic hyperthermia applications [27].

Metastasis is a phenomenon that makes cancer more advanced and its treatment more challenging. Among all cancer treatment methods, treating peritoneal metastasis is significantly more difficult than treating gastric cancer, as the success rate for treating peritoneal metastatic cancer is much lower than that of gastric cancer. Therefore, the tumor's location plays a crucial role in the treatment of this type of cancer. In individuals with significant abdominal adiposity who suffer from gastric cancer accompanied by peritoneal metastasis, the effectiveness of various therapeutic approaches is often reduced, making treatment more difficult and challenging. This reduced efficacy is largely attributed to hormones secreted by adipose tissue, which contribute to treatment resistance in obese cancer patients [28, 29].

This study presents a comprehensive modeling of magnetic nanoparticle hyperthermia for the treatment of cancer originating in the stomach and subsequently metastasizing to the peritoneum. It examines the effects of tumor location (pre- and post-metastasis) and abdominal fat content on the efficiency of the therapeutic process. The primary objective is to achieve a uniform temperature distribution within the tumor, ensuring the complete eradication of cancer cells while preserving the integrity of surrounding healthy tissues. Furthermore, the study evaluates the therapeutic potential of magnetic nanoparticle hyperthermia in addressing peritoneal metastases and investigates how tumor positioning and visceral fat influence magnetic field distribution and heat generation during treatment. Numerical simulation models and advanced engineering techniques are employed to conduct an in-depth analysis of the hyperthermia process and to propose targeted optimizations to enhance its clinical effectiveness.

The innovation of this study lies in the use of numerical models to precisely analyze the distribution of magnetic fields and heat generation in peritoneal tumors. The distribution of magnetic fields and the heat generated within the tumor and surrounding tissues has been carefully examined, as it plays a crucial role in the treatment process. This study specifically analyzes the effects of tumor location and abdominal fat on treatment effectiveness, an issue that has received limited attention in previous research. Additionally, the impact of abdominal fat on treatment efficacy, unlike in other

methods such as radiotherapy, has been thoroughly investigated, especially in obese individuals, where this factor significantly influences treatment outcomes. The practical implications of this research could be valuable in clinical applications, particularly for patients with high abdominal fat who often face challenges with conventional treatments.

This research can play a significant role in designing more precise, effective, and less harmful treatment protocols for peritoneal metastases and other types of tumors. Since the treatment of peritoneal metastases is one of the major challenges in gastric and other organ cancers, the findings of this study can contribute to providing more effective solutions for patient care. Especially in patients with high abdominal fat, this therapeutic approach may offer greater advantages compared to conventional treatments such as chemotherapy and radiotherapy. This study could be a step forward in advancing targeted and less invasive therapies for advanced cancers.

MATHEMATICAL MODEL

Fig. 1 is an image of the geometry of the model. As can be seen, the model that was studied is a two-dimensional (2D) model that includes an induction coil, abdominal tissue, and a spherical tumor in the gastric tissue that eventually metastasizes into the peritoneum. Therefore, AMF is applied to the target tissue (the tumor), and the MNPs in the tumor act as a source of heat generation.

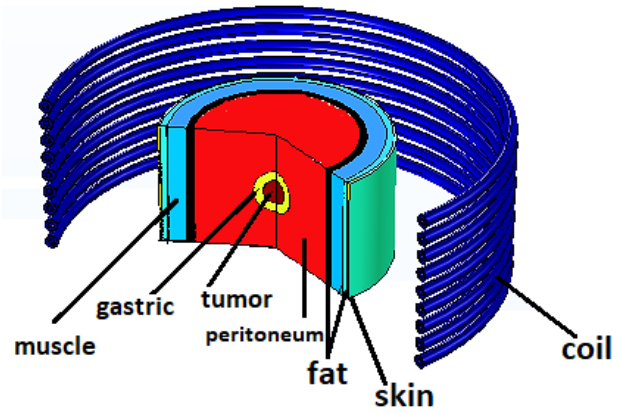


Fig. 1. View of the geometrical model used for MHT.

Model Assumptions

1. The system is linear, isotropic, and stationary.
2. All materials are non-magnetic and have no net electric charge except MNPs inside the tumor.
3. The displacement current density is neglected, and the electric current distribution inside the coil is assumed to be uniform.
4. The system has rotational symmetry around the z-axis.
5. The distribution of MNPs in the tumor is uniform.

Basic Equations

a) Induction Heating

In the process of induction heating, the alternating current in the coil generates time-dependent electromagnetic fields in the space around the coil. When a workpiece or electrically conductive object is placed in these fields, eddy currents are generated, and the Joule effect (RI^2) causes heat to be generated [30, 31].

b) Heat Generated by MNPs

Heat generation by MNPs is obtained as follows [32]:

$$\boldsymbol{P = \mu_0 \pi \chi_0 f H^2 \frac{2\pi f \tau_{eff}}{1+(2\pi f \tau_{eff})^2}} \quad (1)$$

where P, μ_0,χ_0, f, and H are the power dissipation of MNPs per unit volume, the permeability of free space, equilibrium susceptibility, the frequency of the applied magnetic field, and the magnetic field intensity, respectively.

The effective relaxation time in (1), τ_{eff}, can be described as follows:

$$\tau_{eff} = \frac{\tau_B \tau_N}{\tau_B + \tau_N} \quad (2)$$

where τ_B is the Brownian relaxation time, τ_N is Néel relaxation time.τ_B is defined as follows:

$$\tau_B = \frac{3\eta V_H}{K_B T} \quad (3)$$

where η, K_B and T are the viscosity of the suspension, the Boltzmann constant, and the absolute temperature of MNPs, respectively.

V_M is the volume of MNPs without including their shell. Because of the MNPs' spherical volume, it is defined as $V_M = \pi D^3/6$.

V_H is the volume of the MNPs with a shell. It is defined as $V_H = \pi(D + 2\delta)^3/6$.

where D and δ are the diameter of MNPs and the thickness, respectively.

The equation for the Néel relaxation time is:

$$\tau_N = \frac{\sqrt{\pi}}{2} \tau_0 \frac{exp(\Gamma)}{\sqrt{\Gamma}} \quad (4)$$

where K_{eff} is the anisotropy constant, τ_0 ($\tau_0 = 10^{-9} s$) is the attempt time, and $\Gamma = \frac{K_{eff} V_M}{K_B T}$.

The equilibrium susceptibility (χ_0) in the Langevin equation expresses it as follows:

$$\chi_0 = \chi_i \frac{3}{\xi}(coth\,\xi - \frac{1}{\xi}) \quad (5)$$

where χ_i and ξ are the initial susceptibility and the Langevin parameter, respectively.

χ_i described as follows $\chi_i = \mu_0 \phi {M_d}^2 V_M / 3K_B T$ and ξ explained as follows:

$$\zeta = \frac{\mu_0 M_d H_0 V_h}{K_B T} \quad (6)$$

where M_d and ϕ are the domain magnetization of suspended MNPs and the volume fraction of MNPs, respectively.

To get the temperature distribution during hyperthermia, using Pennes bio-heat transfer equations for healthy tissue and tumor tissue, the following relationships are used, respectively [33]:

$$\rho_1 c_1 \frac{\partial T}{\partial t} = \nabla.(k \nabla T) + \rho_b c_b \omega_b (T_a - T) + Q_{met} \quad (7)$$

$$\rho_2 c_2 \frac{\partial T}{\partial t} = \nabla.(k\nabla T) + \rho_b c_b \omega_b (T_a - T) + Q_{met} + P \qquad (8)$$

where ρ_1, ρ_2, ρ_b, c_1, c_2, c_b, k, T, T_a, ω_b, Q_{met}, and P are the tissue density, the tumor density, the blood density, the specific heat of the tissue, the specific heat of the tumor, the specific heat of blood, the thermal conductivity of the tissue, the tissue temperature, and the arterial blood temperature, the blood perfusion rate, the metabolic heat source, and the power dissipation of MNPs per unit volume in the tumor, respectively.

The considered boundary conditions for Pennes bio-heat transfer equations are as follows:

1. On the upper and lower boundaries of the desired model, the heat flux is zero ($\frac{\partial T}{\partial n} = 0$).

2. The temperature on the body surface is considered to be 37 °C.

Solving the Equations

In this study, the finite element method (FEM) was used to solve the coupled Maxwell's and Pennes bioheat transfer equations in cylindrical coordinates. Simulations were carried out in COMSOL Multiphysics 6.0, which enables accurate multi-physics coupling and robust numerical solvers.

An irregular unstructured triangular mesh was used to discretize the computational domain. The mesh was refined near the tumor and coil regions to improve numerical accuracy in areas of high gradient (Fig. 2). The final mesh consisted of approximately 22,000 elements, and a mesh convergence study was performed to verify result stability.

The Galerkin residual method was employed as the spatial discretization scheme. This approach minimizes the residuals across each element and ensures stable numerical performance. For the magnetic field problem, a quasi-static approximation (neglecting displacement current) was used, and a direct solver handled the resulting vector potential formulation of Maxwell's equations. The magnetic field intensity and eddy currents were calculated and applied in Rosensweig's theory [32] to determine power dissipation due to the SPIONs.

The steady-state Pennes bioheat equation [33] was then solved using a Newton–Raphson iterative method with a convergence tolerance of 10^{-6} applied to the temperature field. The solution loop was repeated to ensure coupling between magnetic and thermal fields. The boundary conditions were set as follows: (1) zero heat flux at the top and bottom boundaries, and (2) fixed surface temperature of 37 °C on the outer skin. The electromagnetic boundary included current injection into the copper induction coil (9 circular turns with 5 mm thickness) and magnetic insulation on the simulation boundary.

After the SPIONs were uniformly distributed in the tumor, the tissue was exposed to an alternating magnetic field (AMF). The input current to the coil was adjusted to ensure that the minimum tumor temperature reached 41 °C, initiating the thermal destruction of cancer cells. Although magnetic hyperthermia therapy (MHT) sessions typically last 30–60 minutes in clinical settings for gastric and peritoneal cancers, this study assumes a constant treatment time sufficient to reach the therapeutic temperature range (41–46 °C), based on average thermal dose requirements and tissue tolerance [34].

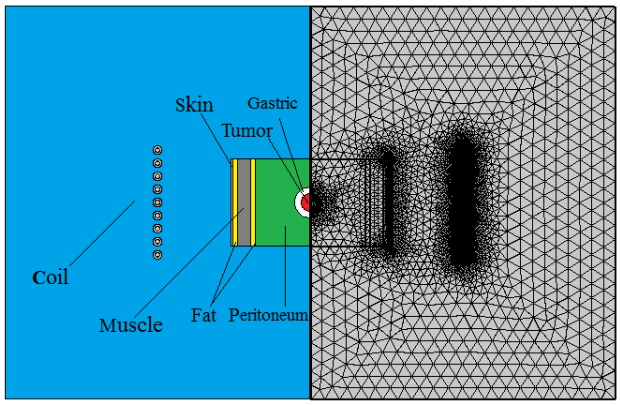


Fig. 2. Computational space (left-hand side) and its mesh for the computation (right-hand side).

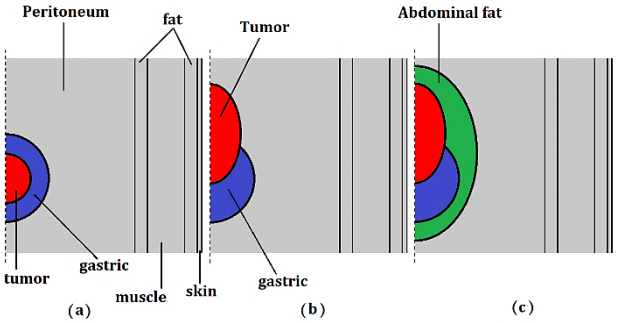


Fig. 3. Location of the gastric tumor, and abdominal fat in the peritoneum: (a) Tumor in the gastric (before metastasis), (b) Peritoneal metastasis, (c) Abdominal fat (after metastasis).

In this study, the geometry dimensions of the model, the thermal characteristics of healthy and tumor tissue used to solve the bio-heat transfer equation, and magnetic and MNPs characteristics are presented in Table 1, Table 2, and Table 3, respectively.

Table 1
Geometry dimensions of the model.

Properties (characteristic)	Value (cm)
Gastric radius	3.5
Peritoneal cavity radius	13
Muscles	3
Extraperitoneal fat and subcutaneous fat	1
Skin	0.4
Outer radius of the cylindrical coil	5
Inner radius of the cylindrical coil	2

Table 2
The thermal characteristics of healthy and tumor tissue used to solve the bio-heat transfer equation [35-38].

Parameters	Blood	Skin	Fat	Muscle	Peritoneum	Gastric	Tumor
Specific heat $(J/Kg.°K)$	3770	3391	2348	3421	3600	3690	3690
Density (Kg/m^3)	1060	1109	911	1090	1055	1088	1088
Thermal Conductivity $(W/m.\ ^{\circ}K)$	0.52	0.37	0.21	0.49	0.51	0.53	0.53
Blood perfusion rate $(1/S)$	-	0.05	0	0.00187	0.018	0.00187	0.002
Metabolic heat (W/m^3)	-	368.1	368.3	1190	5000	1190	31872

Table 3
Magnetic and MNP (Fe_3O_4) properties used in the simulation [10, 31-39].

Parameters	Values	Unit
M_d	446	$kA\ /\ m$
K_{eff}	9	$kJ\ /\ m^3$
τ_0	10^{-9}	S
δ	1	nm
K_B	1.38×10^{-23}	$J\ /\ K$
D	19	nm
f	100	kHz
φ	0/071	-
I	100	A

Grid Independence Test

To ensure that the simulation results are not dependent on mesh resolution, a grid independence test was conducted. Three different mesh densities were used (Table 4).

The variation in maximum temperature across these mesh resolutions was found to be less than 0.5%, indicating that the numerical solution is mesh-independent. Based on this analysis, the medium mesh was selected for all simulations, offering a good balance between accuracy and computational efficiency.

These findings confirm the numerical stability, accuracy, and physical relevance of our computational framework. The consistent alignment with experimental results and the proven mesh independence of the results further support the credibility and applicability of the presented model for hyperthermia treatment planning.

Table 4
Grid independence analysis of maximum tumor temperature

Mesh Type	Elements Number	Maximum Tumor Temperature (°C)
Coarse	~9,000	44.8
Medium	~22,000	44.9
Fine	~47,000	45.0

RESULTS AND DISCUSSION

In this section, the results of magnetic field intensity and distribution, heat generated by nanoparticles, and temperature distribution for the treatment of a human model of peritoneal metastasis cancer are presented. First, the distribution of the external alternating magnetic field and the heat produced by nanoparticles at different tumor locations and various abdominal fat thicknesses are shown. Then, the temperature distribution in the tumor and healthy tissue is discussed. Finally, the effects of tumor location and abdominal fat amount on the heat and temperature distribution in the target tumor have been evaluated. For the calculations, different cases for tumor location are considered, where the tumor starts metastasizing from the stomach and eventually spreads throughout the entire peritoneum. Additionally, the effect of abdominal fat with varying thicknesses (representing individuals with different levels of obesity and abdominal fat) on the treatment process has been studied, as shown in Fig. 3.

Magnetic Field

In Fig. 4 (a, b, and c), the distribution of magnetic field intensity generated by the coil in tumors at different positions is shown, and in Fig. 4 (d, e, and f), the distribution of magnetic field intensity in peritoneal metastasis is presented, considering different abdominal fat thicknesses. As observed, when the tumor is located in the gastric (before metastasis), the maximum magnetic field intensity is at its center. In the case where the tumor has metastasized to the peritoneum, the magnetic field intensity within the cancerous tissue decreases from bottom to top, with its maximum value at the lower part of the tumor, which is closer to the center of the coil (the center of the coil has the highest magnetic field intensity). As it extends upward, the magnetic field intensity in the tumor decreases in that region due to the increasing distance from the center of the coil. Moreover, the magnetic field intensity distribution in the gastric tumor (before metastasis) is more uniform compared to the other cases. In the case of peritoneal metastasis, when the individual has abdominal fat (obesity), the distribution of magnetic field intensity in the tumor does not change with

different abdominal fat thicknesses. This is because the electrical conductivity of fat is much lower (about 0.08%) compared to other tissues (such as the gastric), and therefore, varying amounts of abdominal fat have no significant effect on the distribution of magnetic field intensity.

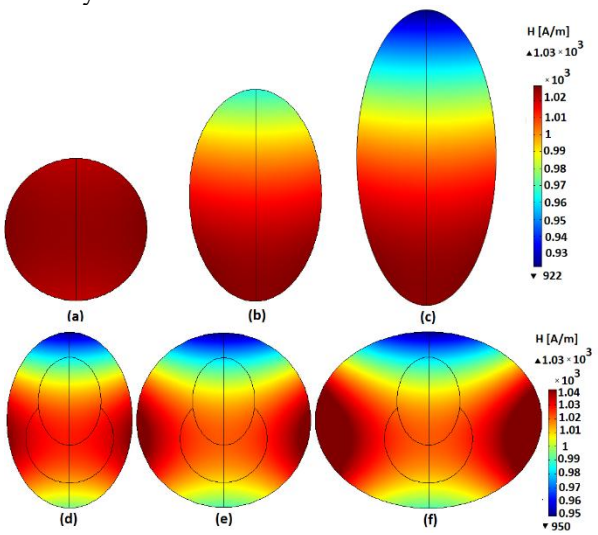


Fig. 4. Magnetic field intensity distribution in the tumor at different locations (Fig. 3 a and b): (a) tumor in the gastric (before metastasis), (b) tumor with 50% peritoneal metastasis, and (c) complete peritoneal metastasis. Magnetic field intensity distribution in peritoneal metastasis tumor, gastric, and abdominal fat (Fig. 3c) with different abdominal fat thicknesses around the stomach: (d) 1 cm, (e) 3 cm, and (f) 5 cm.

Distribution of Heat Generated by Magnetic Nanoparticles in the Tumor

We assume that the nanoparticles are distributed only within the tumor; therefore, the heat generated by the nanoparticles is produced exclusively inside the tumor, which helps preserve the surrounding healthy tissue. Fig. 5 (a, b, and c) shows the heat distribution of nanoparticles in tumors at different locations. Since one of the key factors influencing the heat generated by nanoparticles is the intensity of the magnetic field, and given that the magnetic field intensity is not uniform across different regions of the tumor, the heat distribution also varies depending on the tumor's position. When the tumor is located in the gastric (before metastasis), the maximum magnetic field intensity is centered in the middle of the tumor, resulting in the highest heat generation at the tumor's center. However, in cases of peritoneal metastasis, the magnetic field intensity is greater in the lower part of the tumor compared to the upper regions. Therefore, the maximum heat generation consistently occurs in the lower part of the tumor. The heat distribution generated by nanoparticles for different abdominal fat thicknesses is shown in Fig. 5 (d, e, and f). As observed, abdominal fat has no significant effect on the heat distribution. The total heat generated by nanoparticles in the tumor for the considered cases is presented in Table 5.

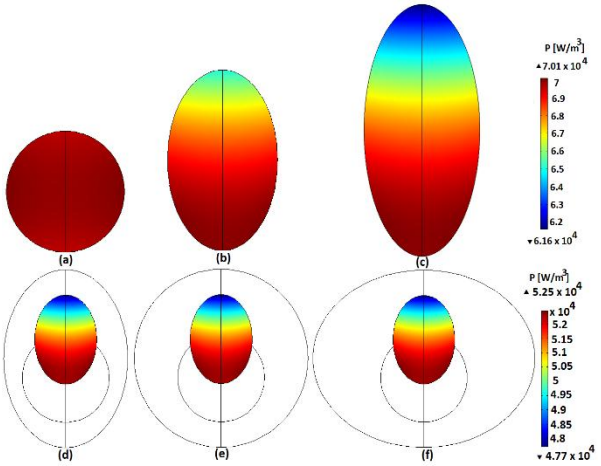


Fig. 5 . Heat distribution of nanoparticles in the tumor at different locations (Figs. 4a and 4b): (a) tumor in the gastric (before metastasis), (b) tumor with 50% metastasis to the peritoneum, and (c) complete peritoneal metastasis. (Fig. 4c) with different diameters of fat around the gastric: (a) 1 cm, (b) 3 cm, and (c) 5 cm.

Table 5
Total heat generated by nanoparticles in the tumor at different locations.

Tumor location	Heat generated by nanoparticles (W)
Gastric	20.3
Tumor with 50% metastasis	31.8
Complete peritoneal metastasis	41.2

Temperature Distribution in the Tumor and Tissue

As previously mentioned, in order to investigate the temperature distribution within the tumor, the results obtained from the power dissipation (nanoparticle heat) were used as input in the Pennes bioheat equation (Equations 6 and 7).

Fig. 6 shows the temperature distribution in the tumor at different locations. The computational results show that the temperature generated in all locations reaches the desired therapeutic temperature range of 41–47°C, and all points within the tumor have temperatures above 41°C, indicating that cancer cells begin to undergo destruction. In all cases, the maximum temperature generated in the tumor is located along the symmetry axis ($r = 0$) and at its central region, with the temperature gradient being symmetric around the tumor center. As we move farther from the central region of the tumor, the temperature decreases due to heat transfer to the healthy tissue and surrounding areas, so that the lowest temperature in all locations is observed on the tumor surface and at the boundary between the tumor and the healthy tissue

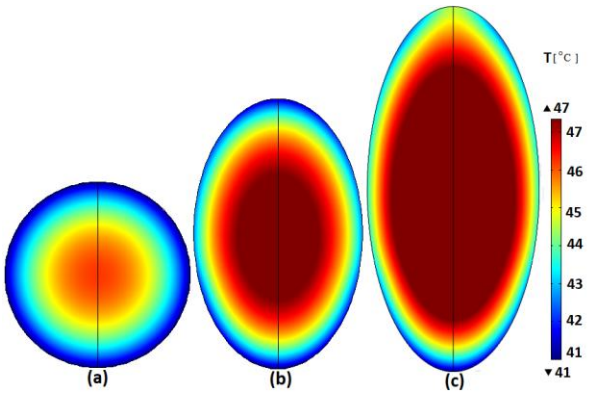


Fig. 6. Temperature distribution in the tumor at different locations (Figs. 4a and 4b): (a) Tumor in the stomach (before metastasis), (b) Tumor with 50% metastasis to the peritoneum, (c) Complete peritoneal metastasis.

With the increase in tumor height (tumor metastasis), the maximum temperature also increases. When the tumor metastasizes, its external surface becomes larger, and the surrounding environment of the tumor changes as well. As the tumor surface area increases, heat transfer to surrounding regions becomes greater, requiring more heat generation to maintain the minimum tumor temperature at 41°C. Therefore, the maximum temperature increases, as shown in Figs. 6 and 7. The main challenges of this treatment method are controlling the localized temperature of the tumor and enhancing the heating efficiency of the nanoparticles [9]. Cancer treatment using magnetic nanoparticle hyperthermia is highly temperature-dependent, such that a temperature variation of just 0.5°C can significantly affect the destruction or survival of cancer cells. The minimum temperature difference between the central and surface regions of the tumor is 4.7°C for the gastric tumor (before metastasis), 6.2°C for 50% peritoneal metastasis (metastasis halfway to the peritoneum), and 7.1°C for complete metastasis. Therefore, the temperature distribution in the tumor before metastasis is relatively more uniform compared to other cases, and as metastasis to the peritoneum occurs and the tumor volume increases, the temperature distribution becomes more non-uniform.

Computational results show that although the temperature in all tumor conditions and locations reaches the desired therapeutic range, the temperature distribution is more uniform and local control is easier in the pre-metastasis stages. Therefore, treatment is simpler and requires less time. For this reason, treating the tumor while it is still confined to the stomach (before metastasis) involves fewer challenges and can be performed more effectively. When the temperature distribution is more uniform, cancer cells throughout the entire tumor are destroyed simultaneously and to the same extent. However, when the temperature distribution is more non-uniform (after metastasis), the center of the tumor, which reaches a higher temperature, is destroyed first, while the remaining parts with lower temperatures require more time for complete destruction, as shown in Fig. 8.

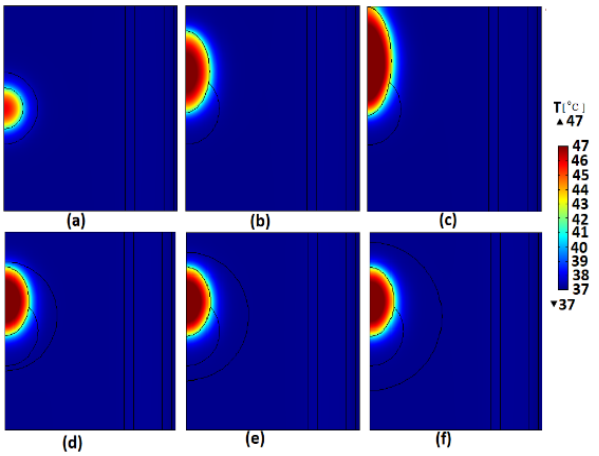


Fig. 7. Temperature distribution in the tumor and healthy tissue at different tumor locations: (a) Tumor in the gastric (before metastasis), (b) Tumor with 50% metastasis to the peritoneum, (c) Complete peritoneal metastasis. abdominal fat with different fat thicknesses around the gastric: (d) 1 cm, (e) 3 cm, and (f) 5 cm

It is important to note that in obese individuals with varying amounts of abdominal fat, conventional treatment methods such as radiotherapy face many challenges and complications compared to other individuals [40]. However, in magnetic nanoparticle hyperthermia, abdominal fat does not affect the treatment process, and the resulting temperature range remains consistent across all different abdominal fat thicknesses, as shown in Fig. 7.

Cancer cells have lower resistance and tolerance to sudden temperature changes compared to healthy tissue; therefore, cancerous tumors can be destroyed. Although this method can raise the internal temperature of cancer cells to the point of cell death, there is also a possibility of other harmful side effects that may affect the surrounding healthy tissues [9]. As shown in Figs. 7 and 8, the temperature of the cancerous tissue falls within the therapeutic temperature range. Now, the potential damage to the healthy tissues adjacent to the tumor must be evaluated. It has been shown that when the temperature exceeds 45°C, tissue damage occurs and cell death takes place [41].

The obtained computational results indicate that the temperature of the healthy tissue surrounding the tumor reaches a maximum of 44.4°C, which implies that no damage is inflicted on the surrounding healthy tissue during the hyperthermia treatment process (Fig. 9).

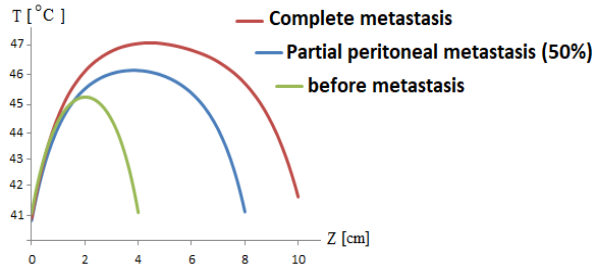


Fig. 8. Temperature distribution plot along the tumor's axis of symmetry at different locations.

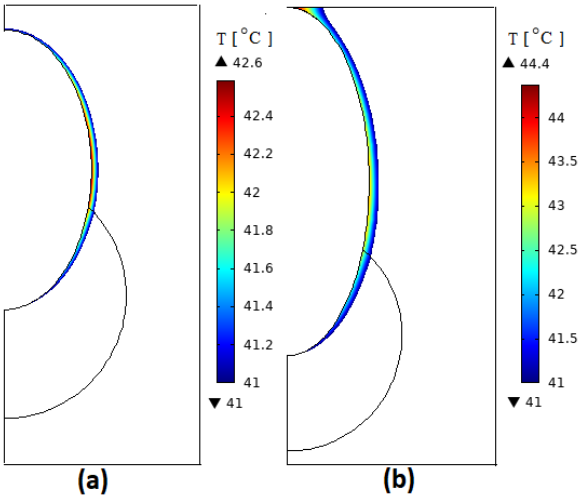


Fig. 9. Temperature distribution of healthy tissue surrounding the tumor in metastatic conditions: (a) partial peritoneal metastasis and (b) complete metastasis.

Discussion and Validation with Experimental Studies

The effectiveness of magnetic nanoparticle hyperthermia (MHT) for the treatment of peritoneal metastasis has been examined in both experimental and clinical contexts by several researchers. In order to validate our numerical findings, we compare our results with experimental data.

Our numerical results, particularly the temperature distribution within tumors and the maximum achievable temperature (ranging from 41°C to 45°C), are in good agreement with experimental findings reported in the literature:

Matsumi et al. [17] demonstrated successful thermal ablation of peritoneal metastases using superparamagnetic iron oxide nanoparticles (SPIONs) under alternating magnetic fields, achieving therapeutic temperatures in the same range as our simulations.

Rouni et al. [22] validated the safety and performance of MHT systems and reported temperature elevation in the torso region consistent with our simulated outcomes.

Chia et al. [23] emphasized the impact of hyperthermia on the tumor immune environment and recorded localized temperature elevations that align closely with our computed thermal fields.

These comparisons suggest that our numerical model accurately captures the essential physics of magnetic hyperthermia and provides realistic predictions for clinical conditions.

The studies conducted by Matsumi et al. [17], Rouni et al. [22], and Chia et al. [23] all highlight the positive effects of magnetic hyperthermia (MHT) in the treatment of peritoneal metastasis. Their findings demonstrate that the use of superparamagnetic iron oxide nanoparticles (SPIONs) can increase tumor temperature, enhance penetration into cancer cells, and lead to a reduction in tumor size. Moreover, this approach enables localized targeting without inducing systemic toxicity. The present study corroborates these findings through numerical simulations, showing that tumor location significantly impacts heat distribution and treatment efficiency. Our results indicate that optimizing these factors can considerably enhance the effectiveness of hyperthermia therapy. In this study, we successfully achieved the therapeutic temperature range of 41 to 45°C, which is sufficient for cancer cell destruction. The study by Rouni et al. focuses on the validation of magnetic hyperthermia systems, employing a combination of experimental measurements and numerical modeling to analyze the distribution of the alternating magnetic field (AMF) and temperature rise in the torso region of patients. Their results, which show a strong correlation between simulated and clinical data, further validate the accuracy of our computational models. These findings play a crucial role in improving the design of magnetic hyperthermia systems, enhancing treatment efficacy, and ensuring patient safety. Additionally, the study by Chia et al. examines the effects of hyperthermia on the tumor immune microenvironment and the biomechanical properties of tumor tissue. Their findings suggest that elevated temperatures can enhance immune cell infiltration into tumors, which may improve treatment outcomes. Our study also confirms this effect by comparing clinical data with simulation results. Previous studies, along with our findings, indicate that magnetic nanoparticle hyperthermia is an effective and safe treatment approach for peritoneal metastasis. This study investigates the impact of environmental factors such as tumor location within the peritoneum and the amount of abdominal fat on the performance of magnetic nanoparticle hyperthermia. By focusing on physical and biological modeling along with advanced simulations, this research analyzes how these factors influence heat distribution and treatment efficacy. The results demonstrate that parameters such as tumor position and fat distribution can significantly affect the effectiveness of hyperthermia, and optimizing the treatment process with regard to these variables can enhance its overall efficiency. The integration of these findings, emphasizing the effectiveness of hyperthermia and the role of environmental factors, can contribute to the development of optimized therapeutic strategies for peritoneal metastasis. However, further research is required to optimize treatment parameters, assess its impact on different cancer types, and explore its integration with combination therapies such as chemotherapy and immunotherapy. Future studies should focus on advanced numerical modeling, extensive clinical measurements, and in-depth biological mechanism investigations to further refine and enhance this therapeutic approach.

CONCLUSIONS

This study examined the impact of various tumor locations and abdominal fat content on the distribution of magnetic field intensity, heat generation, and temperature during the magnetic nanoparticle hyperthermia process. The governing equations of the

system were solved using the finite element method in cylindrical coordinates. The results obtained from the numerical calculations showed that:

1. The magnetic field generated by the induction coil is more uniformly distributed in the case of a tumor before metastasis. The highest magnetic field intensity is observed in cases of full peritoneal metastasis, while the lowest is found in cases of a gastric tumor before metastasis. The amount and thickness of abdominal fat have no effect on the magnetic field generated within the tumor.
2. The heat generated by the nanoparticles in the case of a gastric tumor (before metastasis) has a more uniform distribution compared to other tumor locations. The highest amount of heat generation is observed in full peritoneal metastasis, while the lowest is associated with the gastric tumor. Additionally, abdominal fat has no effect on the amount of heat generated.
3. In all cases, the highest temperature is located at the central region of the tumor. Moreover, the temperature field of the tumor in the case of a gastric tumor (before metastasis) shows a more uniform distribution compared to other cases, with smaller temperature differences throughout the tumor. Therefore, treating a patient with a gastric tumor who has not yet developed peritoneal metastasis is easier and involves fewer challenges.
4. It was observed that in all cases, the temperature of all tumor cells reached the required range for destruction (i.e., 41–47°C); therefore, this type of cancer can be treated with this method in all cases. However, treatment is easier in the pre-metastasis stage.
5. The amount of abdominal fat has no effect on the treatment process, and the use of this treatment method is possible for obese individuals just as it is for others.
6. The maximum temperature in the healthy tissue was found to be 44.4°C, indicating that no damage is caused to the healthy tissue adjacent to the tumor.

Funding Information

The authors appreciate the Bu-Ali Sina University for financial support through the Grant number 1002763.

Declarations

Conflict of interest the authors declare that they have no known competing financial interests or personal relationships that could have appeared to influence the work reported in this paper.

REFERENCES

[1] Siege RL, Miller KD, Wagle NS, Jemal A. Cancer statistics. CA Cancer J Clin. 2023;73:17–48.
[2] Sudhakar A. History of cancer: ancient and modern treatment methods. J Cancer Sci Ther. 2009;1:1.
[3] Valastyan S, Weinberg RA. Tumor metastasis: molecular insights and evolving paradigms. Cell. 2011;147:275–292.
[4] Cortés-Guiral D, Hübner M, Alyami M, Bhatt A, Ceelen W, Glehen O, et al. Primary and metastatic peritoneal surface malignancies. Nat Rev. 2021.
[5] Coccolini F, Gheza F, Lotti M, Virzi S, Iusco D, Ghermandi C, et al. Peritoneal carcinomatosis. World J Gastroenterol. 2013;41:6979–6994.
[6] Mohammadali R, Bayareh M, Usefian A. Cancer cell separation using passive mechanisms: a review. Chall Nano Micro Scale Sci Tech. 2021;9:48–62.
[7] Hedayatnasab Z, Abnisa F, Wan Daud W. Review on magnetic nanoparticles for magnetic nanofluid hyperthermia application. Mater Des. 2017;123:174–196.
[8] Darvishi V, Navidbakhsh M, Amanpour S. Heat and mass transfer in the hyperthermia cancer treatment by magnetic nanoparticles. Heat Mass Transf. 2022;58:1029–1039.
[9] Peiravi M, Eslami H, Ansari M, Zare-Zardini H. Magnetic hyperthermia: potentials and limitations. J Indian Chem Soc. 2022;99:100269.
[10] Rajan A, Sahu NK. Review on magnetic nanoparticle-mediated hyperthermia for cancer therapy. J Nanopart Res. 2020.
[11] Avugadda SK, Fernandez-Cabada T, Soni N, Cassani M, Mai BT, Chantrell R, et al. Magnetic nanoparticles and clusters for magnetic hyperthermia: optimizing their heat performance and developing combinatorial therapies to tackle cancer. Chem Soc Rev. 2021;50:11614–11667.
[12] Johannsen C, Thiesen B, Wust P, Jordan A. Magnetic nanoparticle hyperthermia for prostate cancer. Int J Hyperthermia. 2010;26:790–795.
[13] Golneshan AA, Lahonian M. Diffusion of magnetic nanoparticles in a multi-site injection process within a biological tissue during magnetic fluid hyperthermia using lattice Boltzmann method. Mech Res Commun. 2011;38:425–430.
[14] Lahonian M, Golneshan AA. Numerical study of temperature distribution in a spherical tissue in magnetic fluid hyperthermia using lattice Boltzmann method. IEEE Trans Nanobiosci. 2011;10:262–268.
[15] Adhikary K, Banerjee M. A thermo fluid analysis of the magnetic nanoparticles enhanced heating effects in tissues embedded with large blood vessels during magnetic fluid hyperthermia. J Nanoparticles. 2016:1–18.
[16] Liu W, Chen X. Numerical analysis of electromagnetically induced heating and bioheat transfer for magnetic fluid hyperthermia. IEEE Trans Magn. 2015;51:1–4.
[17] Matsumi Y, Kagawa T, Yano S, Tazawa H, Shigeyasu K, Takeda S, et al. Hyperthermia generated by magnetic nanoparticles for effective treatment of disseminated peritoneal cancer in an orthotopic nude-mouse model. Cell Cycle. 2021;20:1122–1133.
[18] Shoshiashvili L, Shamatava I, Kakulia D, Shubitidze F. Design and assessment of a novel biconical human-sized alternating magnetic field

coil for MNP hyperthermia treatment of deep-seated cancer. Cancers. 2023;15:1672.
[19] Attaluri A, Jackowski J, Sharma A, Kandala SK, Nemkov V, Yakey C, et al. Design and construction of a Maxwell-type induction coil for magnetic nanoparticle hyperthermia. Int J Hyperthermia. 2020;37:1–14.
[20] Bobade RS, Yadav SK. Lateral forces in the helical compression spring. Int J Res Appl Sci Eng Technol. 2017;98.
[21] Misron N, Ying LQ, Firdaus RN, Abdullah N, Mailah NF, Wakiwaka H. Effect of inductive coil shape on sensing performance of linear displacement sensor using thin inductive coil and pattern guide. Sensors. 2011;11:10522–10533.
[22] Rouni MA, Shalev B, Tsanidis G, Markakis I, Kraus S, Rukenstein P, et al. A validated methodological approach to prove the safety of clinical electromagnetic induction systems in magnetic hyperthermia. Cancers. 2024;16:621.
[23] Chia DK, Demuytere J, Ernst S, Salavati H, Ceelen W. Effects of hyperthermia and hyperthermic intraperitoneal chemoperfusion on the peritoneal and tumor immune contexture. Cancers. 2023;15:4314.
[24] Dev K, Kadian A, Manikandan V, Pant M, Mahapatro AK, Annapoorni S. Annealing influence on the magnetic and thermal stability of FeNi3 nanoparticles for magnetic hyperthermia applications. Mater Today Commun. 2025;43:111669.
[25] Singh A, Kumar P, Pathak S, Jain K, Garg P, Pant P, et al. Tailored nanoparticles for magnetic hyperthermia: highly stable aqueous dispersion of Mn-substituted magnetite superparamagnetic nanoparticles by double surfactant coating for improved heating efficiency. J Alloys Compd. 2024;976:172999.
[26] Salati A, Ramazani A, Kashi MA. Tuning hyperthermia properties of FeNiCo ternary alloy nanoparticles by morphological and magnetic characteristics. J Magn Magn Mater. 2020;498:166172.
[27] Litewka JD, Łazarczyk A, Hałubiec P, Szafrański O, Karnas K, Karewicz A. Superparamagnetic iron oxide nanoparticles—current and prospective medical applications. Materials. 2019;12:617.
[28] Iyengar NM, Gucalp A, Dannenberg AJ, Hudis CA. Obesity and cancer mechanisms: tumor microenvironment and inflammation. J Clin Oncol. 2016;34:4270–4276.
[29] Park J, Morley TS, Kim M, Clegg DJ, Scherer PE. Obesity and cancer: mechanisms underlying tumour progression and recurrence. Nat Rev Endocrinol. 2014;10:455–465.
[30] Shokri AJ, Tavakoli MH, Sabouri Dodaran AA, Akhoundi Khezrabad MS. Numerical study of the influence of coil step on the induction heating process in three-dimensional. J Appl Electromagn. 2016;4:37–44.
[31] Tavakoli MH, Karbaschi H. Numerical study of influences of the input current frequency on the induction heating process. Prog Phys Appl Mater. 2021;1:44–49.
[32] Rosensweig RE. Heating magnetic fluid with alternating magnetic field. J Magn Magn Mater. 2002;252:370–374.
[33] Pennes HH. Analysis of tissue and arterial blood temperatures in the resting human forearm. J Appl Physiol. 1948;93.
[34] Dürr S, et al. Magnetic nanoparticles for cancer therapy. Nanotechnol Rev. 2013;2:395–409.
[35] Shokri AJ, Heidari H. Numerical study of the role of nanoparticles in breast tumor treatment in 3D. Prog Phys Appl Mater. 2025;5:23–30.
[36] Rezaeian M, Sedaghatkish A, Soltani M. Numerical modeling of high-intensity focused ultrasound-mediated intraperitoneal delivery of thermosensitive liposomal doxorubicin for cancer chemotherapy. Taylor & Francis. 2019;26:898–917.
[37] Leeuwen RV. Development of an accurate temperature model for intraperitoneal hyperthermia [master's thesis]. Engineering Physics. 2021.
[38] Liu K, Wang C, Cheng PJ. Nonlinear behavior of thermal lagging in laser-irradiated layered tissue. Adv Mech Eng. 2013.
[39] Tang Y, Jin T, Flesch RCC, Gao Y. Improvement of solenoid magnetic field and its influence on therapeutic effect during magnetic hyperthermia. J Phys D Appl Phys. 2020.
[40] Lee K, Kruper L, Dieli-Conwright CM, Mortimer JE. The impact of obesity on breast cancer diagnosis and treatment. Curr Oncol Rep. 2019;21:1–6.
[41] Schooneveldt G, et al. Clinical validation of a novel thermophysical bladder model designed to improve the accuracy of hyperthermia treatment planning in the pelvic region. Int J Hyperthermia. 2018;35:383–397.